MATEC Web of Conferences **16**, 01003 (2014)
DOI: 10.1051/matecconf/20141601003

Modeling and analysis of a horizontally-aligned energy harvester

M. Bendame[1,a], M. Soliman[2], and E. Abdel-Rahman[1]

[1] University of Waterloo, 200 University Avenue, Waterloo, Ontario, Canada
[2] Electronics Research Institute, Giza, Egypt

Abstract. In this paper we analyse an impact-type vibration energy harvester. In this study, the harvester is positioned so that the electromagnetic transducer moves along a horizontal linear guide when subjected to base excitations. The governing equation is a nonsmooth second order differential equation which cannot be solved analytically. Therefore, the averaging method is used to investigate its response. Experimental results are compared with the analytical solution to validate it. The results show that the existence of the nonlinearity in the system enables harvesting at low frequencies, increase the bandwidth, and enhances the output power significantly.

1 Introduction

With advances in the IC, MEMS, and wireless telecommunication technologies, electronic devices such as wireless sensors, portable, biomedical, and wearable electronic devices are getting smaller in size and their power consumption has decreased significantly (a range of wireless devices with different amplitudes of power consumption and typical battery life are shown in Table 1 [1]). At the same time a large number of applications where such devices are used are either placed in remote locations or implanted in areas that are not easily accessible. Most of these low power devices rely heavily on electrochemical batteries as a source of power. Modern battery technologies offer a relatively high specific energy density at a low cost. However, the drawback to battery power is that they have a limited life span and they constantly need to be recharged or replaced. For certain applications, such as wireless sensing and remote monitoring, replacing batteries or recharging them can be expensive, challenging or impossible in some cases. Examples include devices implanted in the human body, devices intended for long duration, and systems that are physically remote [2]. Another serious problem with batteries is the fact that they contain hazardous chemical materials that are harmful to the environment if not recycled. For instance, in Canada over 600 million primary consumer batteries were used in 2007 and about 90% of them end up in landfills [3]. With the world's growing reliance on wireless and low power devices and a push for a green environment, there is a great need for self-powering and self-sustaining low power electronic devices.

The low power design trends combined with self-sustainability needs have opened a new horizon for researchers to look for new ways to power such devices and reduce dependency on batteries. One promising avenue to achieve this goal is to exploit ambient vibration energy sources in order to provide an environmentally friendly and a durable source of energy. Vibration energy harvesting technology has been making significant strides over the last few years as it aims to provide a solution to the aforementioned problem. While the idea of converting vibration into electrical power has been used before, advances in micro-electronics and low power consumption of silicon-based electronics have given it an added significance.

Table 1. Selected battery-operated systems.

Device Type	Power Consumption	Duration
Smartphone	1 W	5 h
MP3 Player	50 mW	15 h
Hearing aid	1 mW	5 days
Wireless sensor	100 μW	Lifetime
Cardiac pacemaker	50 μW	7 years
Quartz watch	5 μW	5 years

2 Vibration energy harvesters

Vibration energy harvesters (VEHs) are used to extract kinetic energy from ambient sources and transform it into electrical energy to power ultra low power electronic devices [4][5]. Over the last few years, a wide range of VEHs have been proposed and demonstrated. Most of the proposed designs employ linear oscillators (spring-mass-damper systems) as the harvesting element. When the seismic mass of the VEH is subjected to base excitations, it oscillates until it attains maximum velocity, and thus input kinetic energy, in a frequency band around its natural frequency defined as:

$$\omega = \sqrt{\frac{k}{m}}, \tag{1}$$

where k is the linear stiffness of the spring and m is the effective mass of the oscillator.

[a] e-mail: mbendame@uwaterloo.ca

While these types of energy harvesters are capable of generating electrical energy with output power on the order of milli-Watts [4][6], their natural frequency must be tuned to match the frequency of ambient vibrations. These harvesters are designed to operate at a single frequency. A high Q-resonance means very limited practical bandwidths over which energy can be harvested [8]. In environments where ambient vibrations are only available at randomly low frequencies, linear harvesters prove to be ineffective because of their high center frequencies and low bandwidth. To overcome these limitations a number of approaches have been suggested. Adaptive kinetic energy harvesters, for instance, use mechanisms to adjust or tune the resonant frequency of the harvester so that it matches the frequency of the ambient vibration and/or widen its bandwidth. Another approach is resonant frequency tuning which can be achieved by changing the mechanical parameters of the structure while widening the bandwidth can be achieved by employing an array of structures with different resonant frequencies [8]. A new approach that has been investigated in recent years is the use of nonlinear dynamical systems and their properties in order to widen the frequnecy band of operation and enhance the harvested power [11][10]. In this paper, we analyze a new type of nonlinear VEH that uses a double-impact oscillator as its harvesting element. Specifically, we study the response of the horizontally aligned configuration of the VEH experimentally and analytically.

2.1 Double-impact VEH

The nonlinear VEH consists of an electromagnetic transducer and a double-impact oscillator. The inertial mass comprised of four magnets and a steel cage, two end limiters consisting of two springs at each end of the housing unit. The carriage moves along the linear guide carrying the assembly with respect to a stationary concentric coil in response to base excitations, as shown in Figure 1. The motion of the magnetic carriage induces a voltage V across the coil terminals that is proportional to the time rate of change of the magnetic flux within the coil [8];

$$V = \frac{d\phi}{dx}\frac{dx}{dt} \tag{2}$$

where ϕ is the total magnetic flux and x is the displacement of the magnetic field (carriage) with respect to the coil. The horizontal implementation of the VEH, shown in Figure 1, is suitable for environments where motions are predominantly in the horizontal direction. The linear guide allows the carriage to move between the two end limiters along the rail while baring motion in other directions [9]. In this configuration, the equation of motion of the horizontally-aligned harvester is given by:

$$m\,\ddot{x} + (b_e + b_m)\,\dot{x} + F(x) = -m\,\ddot{y} \tag{3}$$

where x and y are the displacements of the seismic mass m and the frame, respectively, and $F(x)$ is a nonsmooth function representing the restoring force of the end springs. The VEH harvests kinetic energy transmitted to it from the host vibrations represented by the base acceleration

$$\ddot{y} = A_\circ \cos \Omega\, t \tag{4}$$

where $A_\circ$ and Ω are the amplitude and frequency of the external excitation. The two identical springs are used as limiters on either end of the linear guide. The origin of the coordinate system used to describe the seismic mass is placed at the half point between the springs. The seismic mass m is assumed to be a point mass, as shown in Figure 2. The free distance along the rail (not occupied by the cage) between the upper and lower uncompressed springs is denoted L. The uncompressed length of each spring is denoted x_s and the fully compressed length is denoted x_c. The restoring force, $F(x)$, is represented by a piecewise nonlinear function in terms of linear and nonlinear stiffness of the springs and is written as follows:

$$F(x) = \begin{cases} 0 & -x_s \le x \le x_s \\ k_1(x - x_s) & x_s < x \le x_c \\ k_2(x - x_c) + k_1(x_c - x_s) & x_c < x \le \frac{L}{2} \\ k_1(x + x_s) & -x_c < x < -x_s \\ k_2(x + x_c) + k_1(x_s - x_c) & -\frac{L}{2} \le x \le -x_c \end{cases} \tag{5}$$

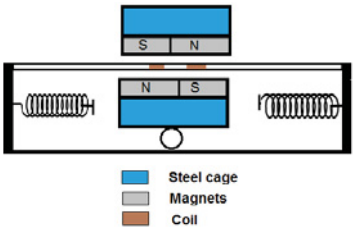

Fig. 1. Schematic of horizontally-aligned VEH

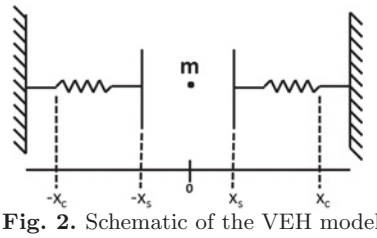

Fig. 2. Schematic of the VEH model

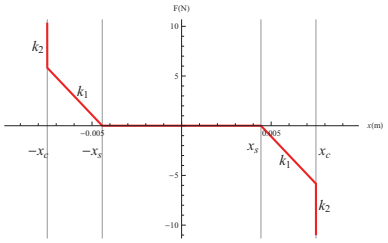

Fig. 3. Force-displacement relationship

where k_1 is the linear spring stiffness and $k_2 >> k_1$ is the stiffness of the fully compressed springs. The force-displacement relationship is shown in Figure 3. When the seismic mass fully compresses the springs, the stiffness changes to that of a very hard spring k_2.

2.2 Magnetic field FEM model

One of the main elements of the electromagnetic VEH is the magnetic flux density. It is therefore important to accurately to design the magnetic circuit with the objective to maximize the flux density around the coil. The magnetic circuit of the VEH is shown in Figure 4, it consists of four magnets arranged as shown in the figure, a steel cage, and an air gap separating the two sets of magnets. The material for the steel cage is mild steel and the magnets are Sintered Neodymium. The

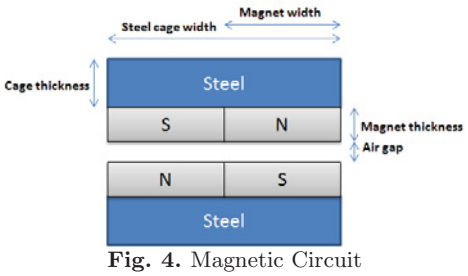

Fig. 4. Magnetic Circuit

finite element modeling software ANSYS was used to determine the magnetic flux density. The FEM simulations results are compared with measured results for validation purposes. The FEM simulation results of the magnetic field strength obtained from ANSYS are shown in Figures 5, 6, while the measured results are shown in Figure 7.

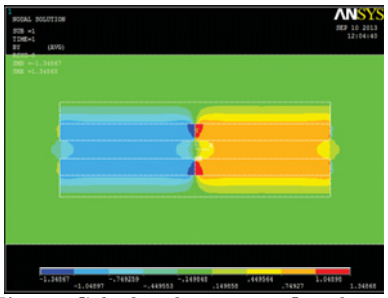

Fig. 5. Calculated magnetic flux density

The measured and simulated results of the magnetic circuit show that the magnetic flux density is constant ($0.74\,T$) in but has opposite signs on each side of the magnetic circuit. This is due to the fact that the polarities of the two sets of magnets are opposite (S-N and N-S). This setup allows the induced voltage across the coil to add up and hence maximize the harvested power.

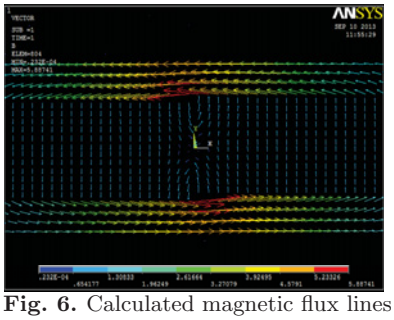

Fig. 6. Calculated magnetic flux lines

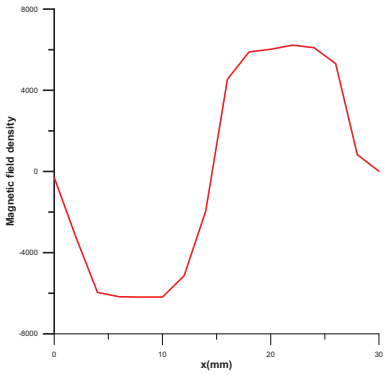

Fig. 7. Measured magnetic flux density

2.3 Electrical damping

The current passing through the coil creates a magnetic field that opposes the field produced by the magnets. The interaction between the two fields produces a force which opposes the motions of the inertial mass. It is this interaction force that acts as electromagnetic damping, and it can be expressed as [9]

$$F_{em} = b_e \frac{dx}{dt} \tag{6}$$

The electrical power is extracted from the mechanical oscillator and is given by [8]

$$P_{em} = F_{em} \frac{dx}{dt} \tag{7}$$

This power is dissipated in the coil resistance R_c and the load resistance R_L. Equating the power dissipated to that generated by the electromagnetic force gives

$$P_{em} = b_e \left(\frac{dx}{dt}\right)^2 = \frac{V^2}{R_L + R_C + j\,\omega\,L} \tag{8}$$

where L is the coil inductance. Substituting for the voltage using equation (2), we can write the electromagnetic damping as

$$b_e = \frac{1}{R_L + R_C + j\,\omega\,L} \left(\frac{d\Phi}{dx}\right)^2 \tag{9}$$

Assuming that the coil inductance is negligible and the magnetic field intensity B is constant, the electromagnetic damping coefficient can be expressed as:

$$b_e = \frac{(Bl)^2}{R_L + R_C} \tag{10}$$

where l is the effective length of the coil. The electrical damping can, therefore, be calculated using Equation (10) and the parameter values given in Table (2).

Table 2. Electromagnetic Transducer Parameters

Parameter	Value
Magnetic Field B (T)	0.7
Effective Coil Length l (m)	0.75
Load Resistance R_L (Ω)	∞ (open-loop)
Coil Resistance R_C (Ω)	2.4

2.4 Mechanical damping

The frequency-response curve of the open-loop harvester is used to determine the quality factor Q of the VEH, defined as:

$$Q_m = \frac{f_0}{\Delta f} \tag{11}$$

where f_0 is the center frequency and $\Delta f = f_2 - f_1$, with f_1 and f_2 are the two half-power frequencies. The quality factor for the open-loop harvester Q_m can then be used to calculate the mechanical damping of the harvester from the following formula;

$$Q_m = \frac{\sqrt{mk_1}}{b_m} \tag{12}$$

where b_m is the mechanical damping coefficient of the open-loop harvester. We can find the mechanical damping using equations (11) and (12) and the values of the systems parameters given in Table (3) as $b_m = 1.12\,\mathrm{kg/s}$. The center frequency and half-power bandwidth were found from a frequency-sweep curve of the base acceleration of the VEH at an amplitude of $A_\circ = 0.05\,\mathrm{g}$ shown in Figure 8. The total damping of the VEH is sum of mechanical damping and electromagnetic damping: $b = b_e + b_m$.

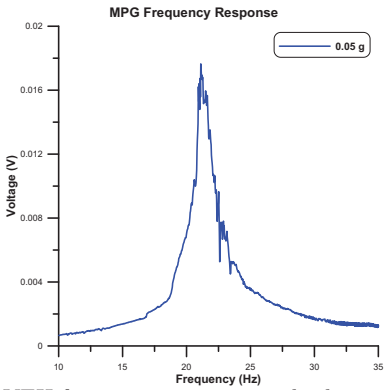

Fig. 8. VEH frequency-response under low excitations

Table 3. VEH Parameters

Parameter	Value
Mass m (kg)	0.12
Stiffness k_1 (N/m)	950
Center Frequency f_0 (Hz)	21

3 Results

In this section we will present the experimental test results of the VEH for different input accelerations. The experimental tests were carried out on the VEH by mounting it on an electromagnetic shaker as shown in Figure 10. A base acceleration was applied as input excitation and the output voltage across the coil terminals with and without load.

3.1 Open-loop transient response

The output voltage of VEH was measured for different input accelerations and and a fixed frequency. The results were recorded and are shown in Figure 9.

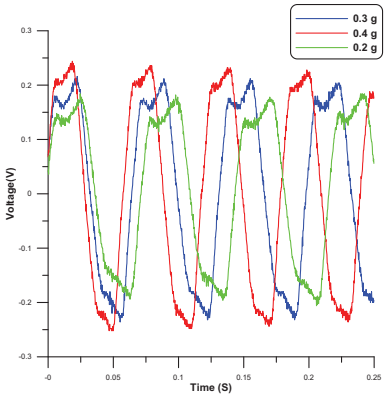

Fig. 9. Time-history of the VEH voltage output for three levels of base excitation

3.2 Open-loop frequency response

The VEH was tested by applying a frequency-sweep of Ω in the range $4\,Hz$ and $25\,Hz$ while holding the amplitude of base acceleration constant $A_\circ$. The VEH was tested for the following inputs: $A_\circ = 0.2$ to $0.4\,\mathrm{g}$ in $0.05\,\mathrm{g}$ increments. Figure 11 shows the frequency-response curves of the RMS voltage for up- and down-sweeps of the different base accelerations.

Test results shown in Figure 11 show that the output voltage of the VEH vary between $100\,\mathrm{mV}$ and $180\,\mathrm{mV}$ for input accelerations varying between $0.2\,\mathrm{g}$ and $0.4\,\mathrm{g}$. We note that the nonlinear center frequencies shift to the right as the input acceleration is increased indicating a type nonlinearity. We also note the existence of sudden jump phenomena and hysteresis in the frequency response curves which indicate the existence of further nonlinearities that could be cubic or possibly quadratic nonlinearities.

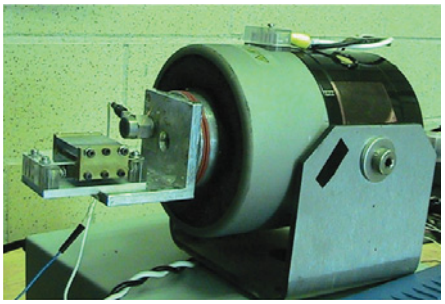

Fig. 10. Test Setup

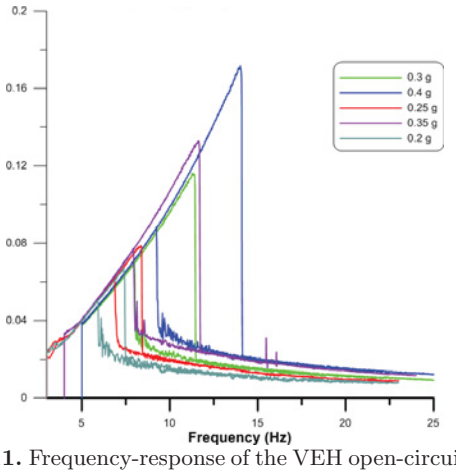

Fig. 11. Frequency-response of the VEH open-circuit voltage for base acceleration amplitudes of $A_0 = 0.2 - 0.4$ g

3.3 Closed-loop VEH frequency response

The closed-loop test was carried out by connecting a load resistor across the coil terminal and measuring its output voltage. Different loads were used during the test to identify the optimum load and therefore the optimum power that can be generated by the harvester. Test results showed that the optimum load varies for different input acceleration.

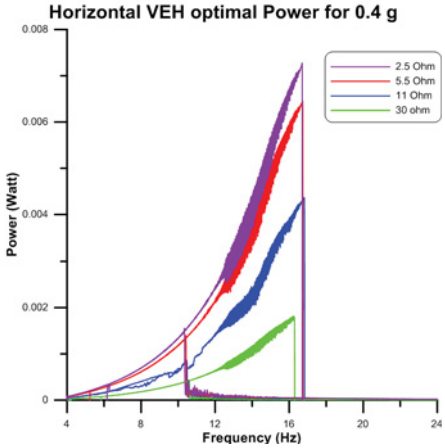

Fig. 12. Frequency-response of the VEH power output for different $R_L = 2.5, 5.5, 11$ and $30\ \Omega$

The closed-loop test results shown in Figure 12 indicate similar nonlinear phenomena to those of the open-loop tests. The existence of hysteresis, jump phenomena and the shifting of the center frequencies as the amplitude acceleration is increased. The maximum voltage of the VEH is approximately 9 mV for an input acceleration amplitude 0.4 g.

4 Analytical solution

The averaging method is used to obtain an approximate closed-form solution of the nonlinear differential equation. In this section we will apply the method to find an approximate periodic solution of the VEH equation of motion given by equation (3). First, the equation is nondimensionalized using the nondimensional variables,

$$\omega_n = \sqrt{\frac{k_1}{m}},\ \omega_h = \sqrt{\frac{k_2}{m}},\ \alpha_1 = \frac{x_s}{L},\ \alpha_2 = \frac{x_c}{L},\\ A = \frac{A_0}{L\,\omega_n},\ \zeta = \frac{b}{2\,m\,\omega_n},\ \gamma = \left(\frac{\omega_h}{\omega_n}\right)^2,\ \Omega = \frac{\omega}{\omega_n}. \tag{13}$$

and is written as,

$$\ddot{x} = A\,\cos(\Omega\,t) - 2\,\zeta\,\dot{x} - F(x) \tag{14}$$

where the nondimensional restoring force is given by:

$$F(x) = \begin{cases} 0 & -\alpha_1 \le x \le \alpha_1 \\ x - \alpha_1 & \alpha_1 < x \le \alpha_2 \\ -\alpha_1 + \alpha_2 + \gamma(x - \alpha_2) & \alpha_2 < x \le 1 \\ \alpha_1 + x & -\alpha_2 \le x < -\alpha_1 \\ \alpha_1 - \alpha_2 + \gamma(\alpha_2 + x) & -1 \le x < -\alpha_2. \end{cases} \tag{15}$$

We assume a solution of the form:

$$x(t) = a\,\sin(\Omega\,t + \beta) \tag{16}$$

where a and β are slowly varying amplitude and phase. We also assume that:

$$\dot{x}(t) = a\Omega\,\cos(\Omega\,t + \beta) \tag{17}$$

subject to the constraint:

$$\dot{a}\,\sin\phi + a\dot{\beta}\,\cos\phi = 0. \tag{18}$$

where we set $\phi = \Omega\,t + \beta$. Using equations (16) and (17) in the equation of motion, equation (3), we obtain the second constraint:

$$\dot{a}\,\cos\phi + 2a\zeta\,\cos\phi + F(x) = \\ a(\dot{\beta} + 1)\,\sin\phi + A\,\cos(\Omega\,t). \tag{19}$$

Solving equations (18) and (19) for $\dot{a}$ and $\dot{\beta}$ yields:

$$\dot{a} = -\big(2a\zeta\,\cos\phi - a\,\sin\phi - A\,\cos(\Omega t) \\ + F(\phi)\big)\,\cos\phi \tag{20}$$

$$a\,\dot{\beta} = \big(2a\,\zeta\,\cos\phi - a\,\sin\phi - A\,\cos(\Omega\,t) \\ + F(\phi)\big)\,\sin\phi \tag{21}$$

Next, we use equation (16) to write the restoring force in terms of the phase angle ϕ as

$$F(\phi) = \begin{cases} 0 & 0 \le \phi \le \phi_1 \\ a\sin\phi - \alpha_1 & \phi_1 \le \phi \le \phi_2 \\ a\gamma\sin\phi + \alpha_2(1-\gamma) - \alpha_1 & \phi_2 \le \phi \le \pi - \phi_2 \\ 0 & \pi - \phi_1 \le \phi \le \phi_1 + \pi \\ a\sin\phi + \alpha_1 & \phi_1 + \pi \le \phi \le \phi_2 + \pi \\ a\gamma\sin\phi + \alpha_2(\gamma-1) + \alpha_1 & \phi_2 + \pi \le \phi \le 2\pi - \phi_2 \\ a\sin\phi + \alpha_1 & 2\pi - \phi_2 \le \phi \le 2\pi - \phi_1 \\ 0 & 2\pi - \phi_1 \le \phi \le 2\pi \end{cases} \tag{22}$$

where

$$\phi_1 = \sin^{-1}\left(\frac{\alpha_1}{a}\right), \quad \phi_2 = \sin^{-1}\left(\frac{\alpha_2}{a}\right)$$

are the phase angles corresponding the seismic mass contacting the linear spring at $x = x_s$ and the fully compressed spring $x = x_c$, respectively.

We define a detuning parameter describing the difference between the forcing frequency Ω and ω_n as

$$\sigma = \Omega - 1$$

and average equations (20) and (21) over the interval of one period $(0, 2\pi)$ to obtain the modulation equations

$$\begin{aligned} \dot{a} =& -\tfrac{1}{2}\zeta a + \frac{A}{2}\cos(\beta - \sigma t) \\ \dot{\beta} =& \frac{1}{2\pi}\left(-2\alpha_2(\gamma-1)\sqrt{1-\frac{\alpha_2^2}{a^2}}\right. \\ & - 2\alpha_1\sqrt{1-\frac{\alpha_1^2}{a^2}} + a(-2(\gamma-1) \\ & \sin^{-1}(\frac{\alpha_2}{a}) - 2\sin^{-1}(\frac{\alpha_1}{a}) \\ & \left. + \pi\gamma)\right) - \frac{1}{2} - \frac{A}{2a}\sin(\beta - \sigma t) \end{aligned} \tag{23}$$

Defining the phase angle $\psi = \beta - \sigma t$, we write the modulation equations in autonomous form as

$$\begin{aligned} \dot{a} =& -\tfrac{1}{2}\zeta a + A\cos\psi \\ \dot{\psi} =& -\sigma + \frac{1}{2\pi}\left(-2\alpha_2(\gamma-1)\sqrt{1-\frac{\alpha_2^2}{a^2}}\right. \\ & - 2\alpha_1\sqrt{1-\frac{\alpha_1^2}{a^2}} + a(-2(\gamma-1) \\ & \sin^{-1}(\frac{\alpha_2}{a}) - 2\sin^{-1}(\frac{\alpha_1}{a}) \\ & \left. + \pi\gamma)\right) - \frac{1}{2} - \frac{A}{2a}\sin\psi \end{aligned} \tag{24}$$

The steady-state periodic solutions correspond to the fixed points (a_0, ψ_0) of the modulation equations. These equations are solved numerically for the fixed points as a function of the detuning parameter σ. Substituting the fixed point at $\sigma = 0$ in the assumed solution form, equation (16), we obtain the seismic mass response shown in 13.

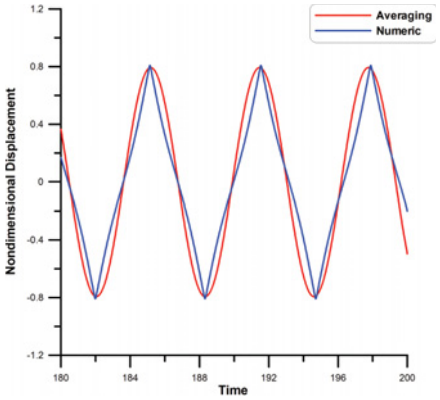

Fig. 13. Displacement of the seismic mass as a function of time obtained numerically (blue) and analytically (red) for base acceleration amplitude of $A_0 = 0.8$ g

5 Conclusion

In this paper we modeled and analyzed the response of a horizontally-aligned low-frequency vibration energy harvester. The VEH was tested experimentally and analytically and results such as optimum power and frequency bandwidth were presented. Results show that the harvester was capable of harvesting low amplitude and low frequency vibrations.

References

1. R.J.M. Vullers, R. van Schaijk, I. Doms, C. Van Hoof, R. and Mertens, "Micropower energy harvesting", Jornal of Solid-State Electronics, Vol. 53, Year 2009, pp. 684-693.
2. D. P. Arnold, "Review of Microscale Magnetic Power Generation", "IEEE Transactions on Magnetics 2009" ,Journal of IEEE Transactrions on Magnetics, Vol. 43, 2007, pp. 3940–3951.
3. `www.ec.gc.ca/gdd-mw/default.asp?lang=En&n=52DF915F-1&offset=1&toc=show`
4. Mostafa S. Soliman, Eihab Abdel-Rahman, E. El-Saadany, R. R. Mansour, "A wideband vibration-based energy harvester", Journal of Micromechanics and Microengineering, Vol. 18, 2008, pp 1257-1265.
5. C. B. Williams and R. B. Yates, "Analysis of a micro-electric generator for Microsystems", Solid-State Sensors and Actuators, Vol. 1, 1996, pp. 369–372.
6. Z. Hadas, M. Kluge, V. Singule and C. Ondrusek, "Electromagnetic Vibration Power Generator", IEEE 2007.
7. P. D. Mitcheson, E. M. Yeatman, "Architectures for Vibration-Driven Micropower generators", Journal of Microelectromechanical Systems, Vol. 13, 2004.
8. S. P. Beepy and T. O'Donnell, Chapter 5, pp. 130–132, in "Energy Harvesting Technology", Eds. S Priya and Daniel J. Inman, Springer, 2009.
9. M. A. E. Mahmoud, E. M. Abdel-Rahman, R. R. Mansour, and E. F. El-Saadany, "Springless Vibration Energy Harvesters", ASME IDETC 2010, Montreal, Canada, August 2010, DETC2010-29046.

10. S. C. Stanton,C. C. McGehee, B. P. Mann. 'Nonlinear dynamics for broadband energy harvesting: Investigation of a bistable piezoelectric inertial generator", Journal Physica D: Nonlinear Phenomena, Vol 239, Pages 640–653, July 2010.
11. Mann, B P and Sims, N D, "Energy harvesting from the nonlinear oscillations of magnetic levitation", Journal of Sound and Vibration, Vol 319, Pages 515–530, July 20096.
12. N. Fondevilla, C. Serre, M. Acero, J. Esteve, and J. Morante, "Electromagnetic Harvester Device for Scavenging Ambient Mechanical Energy With Slow, Variable, and Randomness Nature", PowerMEMS 2009, Washington DC, USA, December 2009, pp. 225-228.
13. A.H. Nayfah and D. T. Mook, "Nonlinear Oscillators", John Wiley, 1997.
14. A.H. Nayfah and B. Balachandran, "Applied Nonlinear Dynamics: Analytical, Computational, and Experimental Methods", John Wiley, 1997.